JOURNAL OF SPACECRAFT AND ROCKETS
Vol. 36, No. 3, May–June 1999

Rarefied Aerothermodynamic Predictions for Mars Global Surveyor

R. G. Wilmoth,* D. F. Rault,† F. M. Cheatwood,‡ and W. C. Engelund‡
NASA Langley Research Center, Hampton, Virginia 23681
and
R. W. Shane§
George Washington University, Hampton, Virginia 23681

Direct simulation Monte Carlo and free-molecular methods are used to provide aerothermodynamic characteristics for the Mars Global Surveyor spacecraft. These characteristics have been used for spacecraft design, mission planning, flight operations, and atmospheric reconstruction. Rarefied transitional flow effects on both heating and aerodynamic drag are shown to be significant. The spacecraft is shown to be aerodynamically stable in both pitch and yaw. The effects of a partially deployed, unlatched solar panel are also studied to provide the aerothermodynamic characteristics of a revised aerobraking configuration. The predictions show that the heating and aerodynamics of this revised configuration are not significantly different from those of the originally planned configuration. Attitude excursions observed in the early aerobraking passes are shown to be explained by significant deflections of the partially deployed panel. The predicted attitudes and panel deflections are in good agreement with flight measurements.

Nomenclature

A_{ref} = reference area, 17.44 m^2 for NASA Langley Research Center three-dimensional model, 16.79 m^2 for direct simulation Monte Carlo analysis code model
C_D = drag coefficient, $D/(\frac{1}{2}\rho_\infty V_\infty^2 A_{\text{ref}})$
C_H = heat transfer coefficient, $\dot{q}/(\frac{1}{2}\rho_\infty V_\infty^3)$
$C_{m,[x,y,z]}$ = moment coefficient about x, y, or z axis, $M_{[x,y,z]}/(\frac{1}{2}\rho_\infty V_\infty^2 A_{\text{ref}} L_{\text{ref}})$
$C_{[x,y,z]}$ = force coefficient in x, y, or z direction, $F_{[x,y,z]}/(\frac{1}{2}\rho_\infty V_\infty^2 A_{\text{ref}})$
$F_{[x,y,z]}$ = force in x, y, or z direction, N
Kn = Knudsen number, λ/L_{ref}
L_{ref} = reference length, 8.73 m
M = Mach number
$M_{[x,y,z]}$ = moment about x, y, or z axis, N-m
n = number density, 1/m^3
q = dynamic pressure, N/m^2
$\dot{q}$ = heat flux, W/m^2
T = temperature, K
V = velocity, m/s
x, y, z = Cartesian body axes, m
α = pitch angle, deg
β = yaw angle, deg
θ = panel sweep angle, deg
λ = mean free path, m
ρ = mass density, kg/m^3

Subscripts

HS = hard sphere
trim = trim condition
∞ = freestream

Introduction

MARS Global Surveyor (MGS) is the first planetary mission designed specifically to use aerobraking as a primary means of customizing its orbit to achieve its science objectives.[1] The feasibility of aerobraking was demonstrated by Magellan near the end of its mission around Venus.[2] However, aerobraking was not a primary initial objective for Magellan, and the aerobraking was not as aggressive as that used for MGS. The MGS prelaunch plan called for a large number of aerobraking passes over a period of about four months to gradually reduce the periapsis velocity by about 1 km/s and transform the highly elliptical capture orbit into the nearly circular orbit needed for atmospheric and surface mapping experiments. MGS was launched on Nov. 7, 1996, reached Mars on Sept. 11, 1997, and began aerobraking on Sept. 17, 1997. After initial orbit insertion, the spacecraft used small propulsive maneuvers to gradually lower its periapsis into the atmosphere, where it uses its solar panels as wings to achieve the necessary aerodynamic drag. Anomalies that occurred during orbits 12–15 caused a temporary halt to the aerobraking phase. After extensive analysis of the status of the spacecraft, a revised aerobraking plan was developed, and aerobraking was resumed on Nov. 7, 1997, and is proceeding smoothly but less aggressively.

The atmospheric densities that MGS encounters place the spacecraft well into the rarefied transitional flow regime during aerobraking (see Fig. 1). The MGS spacecraft goes much deeper into the atmosphere of Mars in comparison to the exploratory aerobraking experiments of Magellan in the Venus atmosphere. Therefore, MGS designers relied heavily on analytical and numerical predictions of aerodynamics and heating to design the spacecraft, to plan the aerobraking operations, and to interpret flight results. Based on prelaunch analyses, a configuration was selected in which both solar panels would be swept backward 30 deg to provide aerodynamic stability together with acceptable drag and heating. This prelaunch configuration was analyzed extensively using free-molecular and direct simulation Monte Carlo (DSMC) techniques to provide comprehensive data on the aerothermal environment for various aerobraking and nonaerobraking geometries, including the effects of

Received Jan. 20, 1998; revision received Aug. 15, 1998; accepted for publication Feb. 22, 1999.

*Aerospace Engineer, Aerothermodynamics Branch, Aero and Gas Dynamics Division. Senior Member AIAA.
†Aerospace Engineer, Aerosol Research Branch, Atmospheric Sciences Division.
‡Aerospace Engineer, Vehicle Analysis Branch, Space Systems and Concepts Division. Member AIAA.
§Graduate Research Scholar Assistant, Joint Institute for Advancement of Flight Sciences. Member AIAA.

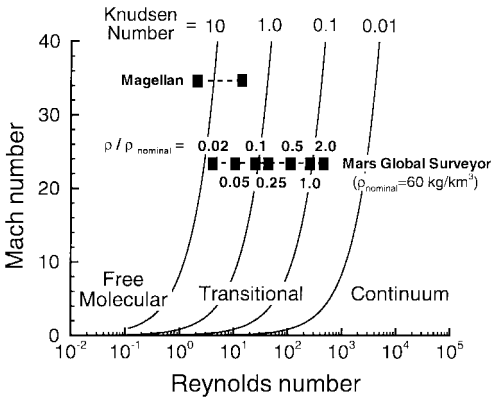

Fig. 1 MGS trajectory in Reynolds–Mach–Knudsen number domain.

reaction control jet firings.[3–5] The prelaunch heating predictions were used by spacecraft designers to design the panel thermal protection, and aerodynamic drag predictions were used by mission planners to optimize the aerobraking trajectories.[3]

Aerodynamic predictions are also important in connection with onboard accelerometer measurements[6] being used for atmospheric reconstruction experiments. These experiments are designed to provide new data on the structure of the Mars atmosphere and to assist mission operations through real-time monitoring of the atmospheric density. Aerodynamic predictions are essential to the atmospheric reconstruction process, and at the same time, knowledge of the atmospheric density allows the predicted aerodynamic and thermal loads to be quantified based on measured flight parameters. Although the aerothermal environment that MGS experiences is relatively benign compared to that encountered by typical hypersonic entry vehicles, the thermal and structural design of the MGS spacecraft is more fragile than the typical entry vehicle, and the predicted aerodynamic and aerothermal loads are significant.

When the MGS solar panels were deployed from their stowed position shortly after launch, one of the panels failed to fully extend into a latched position, resulting in a kink in the panel geometry.[7] Because the panel hinge was not latched, an alternate configuration had to be developed to prevent excessive panel deflections during aerobraking. Therefore, mission planners decided to rotate the panel 180 deg so that aerodynamic forces would tend to push it toward the latched position. Slight alteration of the planned sweep angles for each panel was then needed to provide the proper aerodynamic trim. This revised aerobraking configuration was analyzed to assess its aerothermodynamic properties.

Finally, when MGS began aerobraking in September 1997, the spacecraft experienced unexpected atmospheric density excursions, and the partially deployed solar panel showed evidence of deflecting more than predicted. The interpretation of the behavior of the partially deployed panel depended strongly on predictions of aerodynamic trim position and on predicted aerodynamic hinge loads on the panel. Alternate aerobraking configurations were considered as a possible means for reducing the solar panel hinge loads, and further aerodynamic analysis was required to assess these configurations.

The MGS program is the first planetary mission in which rarefied transitional flow predictions, in particular DSMC, have played such an integral role all of the way from preliminary design through mission operations and flight data analysis. The purpose of this paper is to summarize predictions that have been made for the various purposes just described and to present recent results that have not been previously published. This paper focuses on predictions for the revised aerobraking configuration and in support of flight measurements and interpretation. Also, because different geometry models and computational techniques were used for these more recent studies than for previously published prelaunch predictions, comparisons with the earlier prelaunch predictions are given. The rarefied computational tools, various spacecraft geometry models, and simulation conditions are described, representative heating and aerodynamic predictions are given, and calculations with particular relevance to flight operations and data interpretation are presented. Finally, a limited discussion of flight results is provided. A complete discussion of the accelerometer measurements and mission operations is given elsewhere.[6,8]

Rarefied Aerothermodynamic Analysis Tools

In rarefied transitional flows, molecular collision effects must be taken into account, and the DSMC technique of Bird[9] is the most widely accepted technique to simulate these flows. The motion of thousands to millions of representative molecules are tracked while the molecules undergo collisions among themselves and with any surfaces that may be present. Collisions are typically modeled using the variable hard sphere model developed by Bird with internal energy exchange modeled using the Borgnakke–Larsen model.[10] Surface collisions are generally modeled as a combination of diffuse and specular scattering to represent partial momentum and energy accommodation.

Various computer codes have been developed to implement the DSMC technique and the two codes used for the MGS analyses are the NASA Langley Research Center three-dimensional (LaRC-3D) DSMC code[11] and the DSMC analysis code (DAC).[12] Both codes can handle complex three-dimensional geometries but differ in their treatment of surface geometry and flowfield grids. The LaRC-3D DSMC code uses an unstructured grid, where each computational cell is composed of one or more elements from an underlying uniform Cartesian mesh, which may be made finer near the body. The body geometry is described as a discrete set of small Cartesian elements, but the code retains information on local surface normals from a more exact geometry definition and allows inclusion of a body-fitted grid near the wall to capture Knudsen layers. DAC uses a two-level Cartesian grid, where the first level is a uniform structured mesh and the second level consists of a locally refined Cartesian mesh within each first-level cell. The body geometry is described as an unstructured triangular grid, which clips the local Cartesian grid. Each code has certain unique advantages, but both codes use essentially the same DSMC procedures and physical models, and both are capable of handling the complex geometry of the MGS spacecraft. The LaRC-3D code was used for all of the prelaunch predictions and for several postlaunch analyses of the revised aerobraking configuration. DAC was used mainly to generate the aerodynamic database for the atmospheric density reconstruction[6] and to provide analyses in support of various mission operations.

The DSMC analyses were supplemented by various free-molecular codes. The free-molecular calculations use the standard free-molecular equations given by Bird,[9] and codes have been developed to accept the same three-dimensional geometry descriptions used by the LaRC-3D and DAC and to provide compatible output.[11,12] These codes account for geometric shadowing that occurs in complex geometries and give essentially the same results as the DSMC codes in the collisionless, hypervelocity limit.

Spacecraft Geometry Models

The geometry models used for the prelaunch analysis with the LaRC-3D DSMC code and for the postlaunch analysis with DAC are shown in Fig. 2. The LaRC-3D geometry model (Fig. 2a) is constructed from a highly detailed thermal radiation analysis system (TRASYS) model. The computational model resolution of some components is actually higher than that shown and is reduced in Fig. 2a for convenience of plotting. The TRASYS model contains a more detailed description of the spacecraft bus than that used for the postlaunch configuration with DAC (Fig. 2b). However, the two models have approximately the same projected frontal area, an important parameter for drag predictions in rarefied flows, and the definition of the solar panels is very similar for the two models. The reference areas used to nondimensionalize force and moment coefficients are 17.44 m^2 for the LaRC-3D model and 16.79 m^2 for the DAC model. These reference areas approximately represent the projected frontal area for the prelaunch and postlaunch computational models, respectively, with the solar panels in their nominal aerobraking position. For comparison, the best estimate of

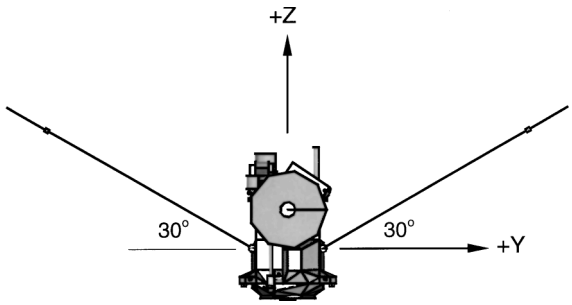

a) Prelaunch aerobraking configuration; TRASYS model for LaRC-3D DSMC code

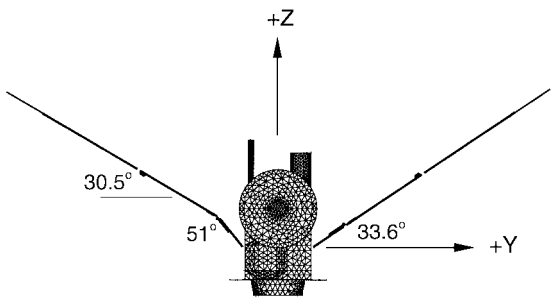

b) Postlaunch revised aerobraking configuration; unstructured grid model for DAC

Fig. 2 MGS geometry models.

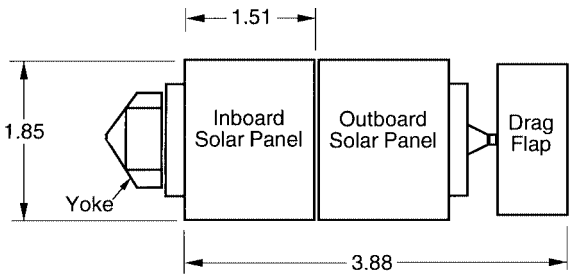

Fig. 3 Schematic of a single MGS solar panel (dimensions in meters).

this frontal area for the actual postlaunch spacecraft based on drawings of the flight hardware is 17.01 m^2. The reference length used for moment coefficients is 8.73 m for all cases and is the approximate distance between the ends of the $+Y$ and $-Y$ outboard solar panels (excluding the drag flap) when both panels are at 30-deg sweep.

A schematic of a single solar panel is shown in Fig. 3 with key components and dimensions labeled. The complete solar panel assemblies make up about 83% of the total projected frontal area of the spacecraft in the nominal aerobraking configuration (panel sweep $\approx$30 deg). The y-shaped yoke is attached to the spacecraft bus through a two-axis gimbal, and the inboard solar panel is attached to the yoke by hinges and a damper. The computational geometry models are constructed so that the yoke, the inboard and outboard solar panels, and the drag flap can be easily rotated into any desired orientation. For the prelaunch configuration, the solar cells (the details of which were not modeled) are assumed to be on the leeward side, whereas for the revised postlaunch configuration, the solar cells on the partially deployed panel are assumed to be on the windward side. Because of material differences between the surfaces of the solar arrays and the composite facesheet to which the arrays are attached, possible differences in gas–surface accommodation coefficients exist between the $+Y$ and $-Y$ panels. The effect of such differences are discussed later.

Simulation Conditions

All calculations presented are for a freestream velocity of 4.811 km/s, which is the nominal value near periapsis. The atmosphere is assumed to be 95.37% carbon dioxide and 4.63% molecular nitrogen by mole at a temperature of 148 K. All surfaces are

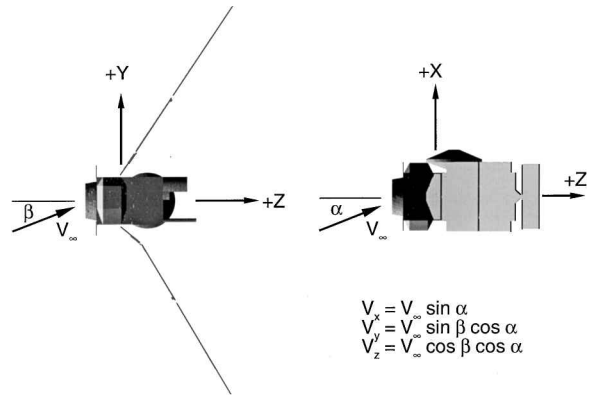

Fig. 4 Definition of pitch α and yaw β in the spacecraft coordinate system; velocity components in x, y, and z directions given in terms of V_∞, α, and β.

assumed to be at a temperature of 300 K and, unless otherwise specified, to have diffuse scattering with full momentum and energy accommodation [accommodation coefficient (AC) = 1.0]. This surface temperature is an upper limit of that typically experienced in flight, i.e., actual temperatures are generally lower, but sensitivity studies show that the aerodynamic forces are not significantly different at the lower temperatures. AC differences between the $+Y$ and $-Y$ panel do have an effect on aerodynamic trim, and those differences are discussed. However, full accommodation is assumed for all heat transfer calculations to give an upper limit on the expected heating for design purposes.

Calculations for both the prelaunch and postlaunch configurations were performed at various attitudes (α and β) and atmospheric densities. Pitch angle α and yaw angle β are defined in the spacecraft coordinate system as shown in Fig. 4. The aerodynamic database generated for density extraction is based on computations at nine different attitudes (α and $\beta = -15$, 0, and 15 deg) for each of three densities ($\rho_\infty = 12$, 60, and 120 kg/km^3) corresponding to the transitional flow regime and for conditions corresponding to free-molecular flow. Computations were also carried out for various sweep angles θ (30.5, 40.5, and 50.5 deg) of the $-Y$ panel to simulate deflections of the unlatched panel. Other calculations were performed at various densities, sweep angles, and attitudes needed to address specific flight issues. Knudsen numbers are based on a constant hard-sphere diameter of 4.64×10^{-10} m for the CO_2/N_2 mixture and a reference length of 8.73 m.

Results

Selected results are presented in the following sections to show the rarefied nature of the atmospheric flow around the MGS spacecraft, the level of heating encountered at various densities, and the aerodynamic drag and stability. Comparisons are made between the prelaunch and postlaunch predictions to show the sensitivity of the aerodynamic predictions to the geometry models and DSMC codes. Results are also shown that illustrate the sensitivity of the aerodynamics to certain modeling parameters. Finally, a limited discussion of various results and their relation to measured flight data obtained during aerobraking is given.

Flowfield

Over the range of atmospheric densities encountered by MGS, the spacecraft flies in what is generally considered rarefied transitional flow. At apoapsis, the atmospheric density is negligible, and the spacecraft is in free-molecular flow. At the lowest periapsis altitude anticipated, the maximum expected atmospheric density was estimated prior to launch to be about 120 kg/km^3 based on existing Mars atmospheric models. At this density, the Knudsen number (ratio of mean free path to reference length) is about 0.07 using the total span of the solar panels (swept at 30 deg) as the reference length. A comparison of the predicted density contours around the MGS spacecraft is given in Fig. 5. At an atmospheric density of 12 kg/km^3 ($Kn \approx 0.7$), the flow is relatively rarefied, and perturbations to the local density field caused by molecules reflecting

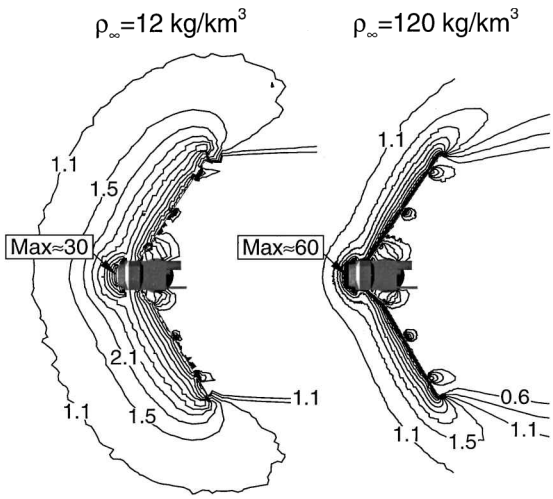

Fig. 5 Density contours ($\rho/\rho\infty$) around MGS at two different atmospheric densities; cut taken in Y–Z plane near middle of solar panels, $\alpha = \beta = 0$.

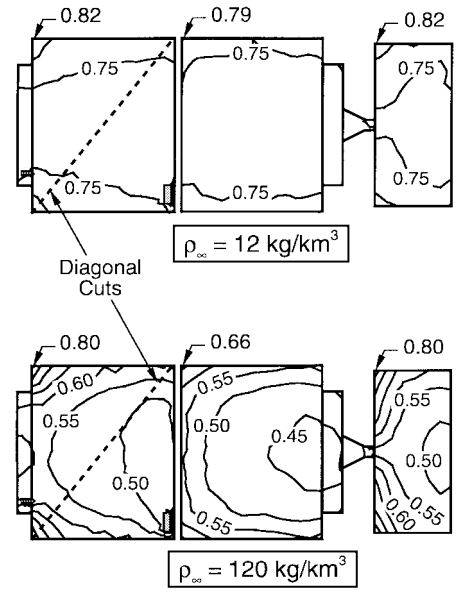

Fig. 6 Heat transfer contours (C_H) on solar panel; view normal to panel, which is at 30.5-deg incidence to flow.

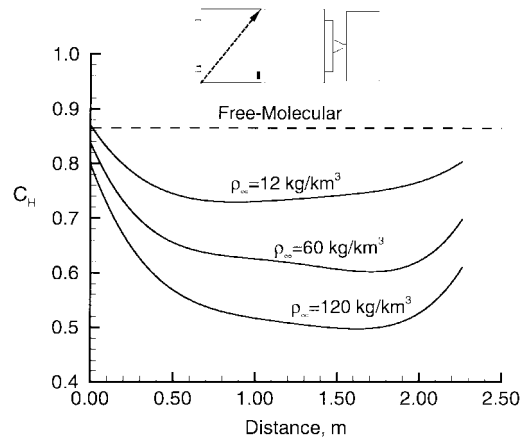

Fig. 7 Heat transfer distribution along diagonal of inboard solar panel; horizontal dashed line is free-molecular limit.

from the spacecraft extend much farther ahead of the body than at 120 kg/km^3 ($Kn \approx 0.07$), where the relative density near the spacecraft is much higher and a weak shock-like structure is evident. However, local densities are high compared to the freestream density in both cases, which demonstrates that local departure from free-molecular conditions is significant. The density reaches values approximately 30 times the freestream density at 12 kg/km^3 and approximately 60 times freestream at 120 kg/km^3. The largest densities occur on the windward side of the spacecraft bus, where the main propulsion nozzle is modeled with a large flat forward-facing surface. However, densities are also high near the surface of the solar panels, which are swept approximately 30 deg. These high densities are caused both by the bluntness of the vehicle and by the low surface temperatures.

Under purely free-molecular conditions, the perturbations to the density field extend farther upstream than indicated in Fig. 5, and local conditions can be viewed as just the linear superposition of conditions based on the uniform freestream molecules and molecules reflected from the surfaces of the spacecraft. The influence of the departure from free-molecular flow (transitional effects) on the heating and aerodynamics is discussed in the following sections.

Heating Predictions

Predictions were needed to design thermal protection for sensitive portions of the MGS spacecraft where the aerodynamic heating would be the most significant. Because the solar panels are directly in the hypervelocity flow during aerobraking and because of the relatively low-temperature limits on the solar cells, rarefied transitional flow calculations focused on heating predictions for the panels at various densities and sweep angles.

Typical surface heating distributions on the solar panels are shown in Fig. 6 as surface heat transfer coefficient C_H contours at freestream densities of 12 and 120 kg/km^3. In Fig. 6, the panel is viewed normal to the surface while the panel is at 30.5-deg incidence to the flow. These particular results were obtained for the revised postlaunch configuration with DAC. At 12 kg/km^3, the heating distribution is relatively uniform, whereas at 120 kg/km^3, the distribution shows significant gradients across the panel with maximum heating near the edges and corners. This transitional effect is caused by the development of the shock layer upstream of the panel that tends to shield the central regions whereas the heating along the outer edges is much closer to that for free-molecular flow. In free-molecular flow, the heating distribution would be uniform on the panel. The results shown are quite similar to those obtained by Rault et al.,[3] on the prelaunch configuration, which were used by spacecraft designers to lay out the panel thermal insulation and protective paints. Heat transfer predictions for nonaerobraking geometries and other spacecraft attitudes are provided by Shane et al.[5]

The heating gradients on the panel are further illustrated in Fig. 7, where C_H is plotted along a diagonal cut across the inboard panel for three different freestream densities. The free-molecular limit is shown as a horizontal dashed line. These gradients are important in the interpretation of temperature measurements in flight because such measurements are used as a real-time indicator of the heat load on the panel during aerobraking.[6] Because the thermocouples are mounted near the center of the panels, it is necessary to know the ratio of the heat transfer at the thermocouple location to that at the edges to have a proper indication of the peak heating condition being experienced. Results such as these were obtained by Shane[13] to essentially calibrate the thermocouple measurements to indicate peak heating on the inboard and outboard panels under a variety of conditions.

In the revised configuration, the back side of the partially deployed $-Y$ panel is facing the flow, and several electronic and instrument assemblies (shunt boxes, sun sensors, etc.) are exposed directly to the flow when the panel is rotated 180 deg for the revised aerobraking configuration described earlier. Therefore, additional calculations were performed to determine whether significant interference effects might be caused by these protuberances. DSMC analyses show that the local mean free path in the vicinity of these various objects is of the same order as their dimensions. Therefore, although these protuberances alter the heating in their near vicinity, local heating either is negligibly increased due to the orientation of the objects or is decreased due to shadowing.

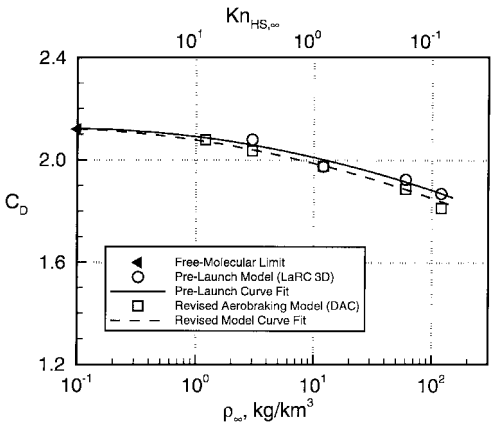

Fig. 8 Drag variation with atmospheric density; solid and dashed lines are curve fits to prelaunch and postlaunch predictions, respectively.

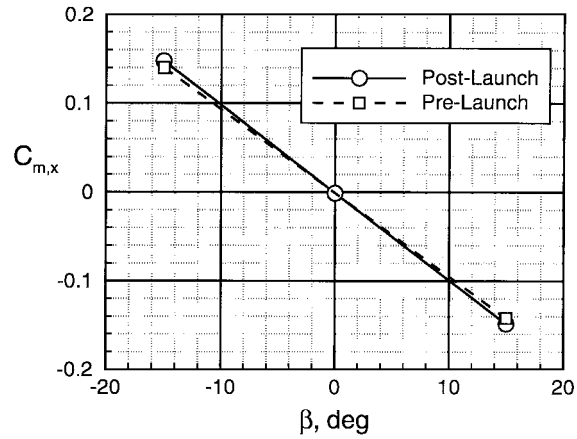

a) Moment coefficient about *X* axis (yaw)

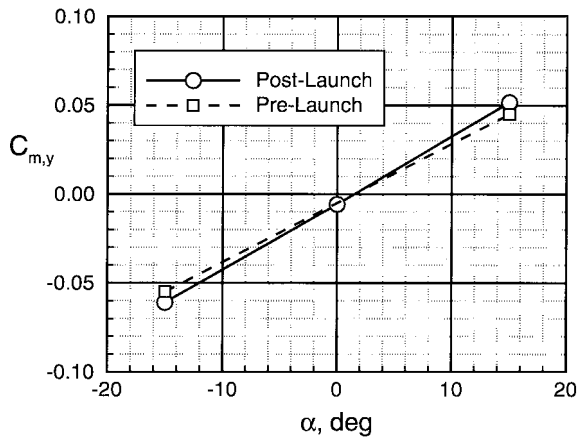

b) Moment coefficient about *Y* axis (pitch)

Fig. 9 Comparison of pitch and yaw moment predictions for prelaunch and postlaunch configurations.

Aerodynamic Predictions

The aerodynamic drag of MGS is a critical parameter in designing the aerobraking mission. The spacecraft must have sufficient drag to provide the change in velocity, ΔV, needed to circularize the orbit in the allotted mission time frame. Transitional flow aerodynamic predictions obtained by Rault et al.[3] for early prelaunch designs were instrumental in the spacecraft designer's decision to add the drag flaps (see Fig. 3) to provide approximately 2.8 m^2 of additional frontal area for aerobraking. These predictions were used by mission planners to optimize the aerobraking trajectories. Static aerodynamic stability predictions were also needed to design the flight controls and were especially important for determining the trim position of the spacecraft with the unlatched panel.

Prelaunch/Postlaunch Comparison

The variation of the drag coefficient with density for the final prelaunch configuration (with drag flaps) and the revised aerobraking flight configuration is shown in Fig. 8. The drag coefficient is approximately 15% lower than the free-molecular value at the highest expected density, and the prelaunch and postlaunch models give approximately the same drag coefficients. The drag coefficients for the revised postlaunch model obtained with DAC are generally lower than those for the prelaunch configuration obtained with the LaRC-3D code. However, quadratic, least-square, curve fits to each set of predictions (shown as solid and dashed lines in Fig. 8) give essentially the same trends, and differences between the two results are less than 2% at the higher densities. These small differences are due to a combination of both physical and simulation factors. The panel sweep angles are slightly different for the two sets of calculations, and the simulations have different geometry representations, grid resolution, and statistical scatter. However, both models give essentially the same free-molecular drag coefficients. Overall, the agreement is quite good.

A comparison of moment coefficients about the X and Y axes is shown in Fig. 9. The origin has been translated to the spacecraft center of mass, so that a moment of zero indicates the aerodynamic trim position about each axis. Also, for the spacecraft coordinate system chosen, a negative slope for $C_{m,x}$ vs β and a positive slope for $C_{m,y}$ vs α indicate positive aerodynamic stability. The prelaunch and postlaunch predictions show very little difference in the magnitude of these moment coefficients, and the trim angles about both the X and Y axes agree to within about 0.1 deg.

Revised Aerobraking Configuration

Aerodynamic database. Postlaunch predictions for the revised aerobraking configuration obtained with DAC are used to generate an aerodynamic database to extract atmospheric density profiles during each aerobraking pass from accelerometer measurements.[6] Because the unlatched solar panel was expected to deflect under aerodynamic load, the aerodynamic coefficients were expected to change due to transitional flow effects and due to geometrical changes both of which would be a function of density. Therefore, the aerodynamic database was expanded to include additional sweep angles of the $-Y$ panel to represent these deflections. The extraction of atmospheric density from measured accelerations then requires an iterative process to account for density variations, attitude variations, and geometrical changes. In addition to providing the overall spacecraft aerodynamics, the rarefied flow simulations provide data on the hinge moments used to calculate the actual deflection of the $-Y$ panel. A complete discussion of the accelerometer data reduction procedure is given in Ref. 6.

The aerodynamic database is summarized in Figs. 10 and 11. Figure 10 shows the drag coefficient under trim conditions in both pitch and yaw as a function of atmospheric density for three sweep angles of the $-Y$ panel. A sweep angle θ of 30.5 deg corresponds to zero deflection, and 40.5- and 50.5-deg sweep correspond to 10- and 20-deg deflections, respectively. Deflection of the $-Y$ panel reduces the projected frontal area, and the drag coefficient (based on the nominal reference area) is lower for panel sweep angles of 40.5 and 50.5 deg than for the nominal sweep. However, transitional flow effects are similar for all three panel sweep angles, and variations with density are well represented by second-order curve fits.

Figure 11 shows the moments about the X and Y axes as a function of pitch and yaw angle for the three panel sweep angles at an atmospheric density of 120 kg/km^3 (results are qualitatively similar for lower densities). As the $-Y$ panel deflects, the trim position about the X axis (Fig. 11a) shifts to values that are almost one-half of the deflection angle (deflection angle $= \theta - 30.5$ deg). However, the trim position about the Y axis (Fig. 11b) is essentially unaffected.

For extraction of atmospheric density from the accelerometer measurements, only the axial force component C_z is used because the data rates for the X- and Y-axis accelerometer components are much lower and less accurate. Further discussion of the use of the aerodynamic predictions in the flight data analysis is given elsewhere.[6]

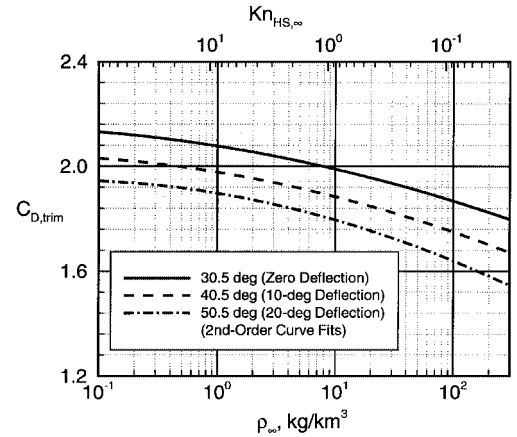

Fig. 10 Effect of $-Y$ panel deflection on trim drag.

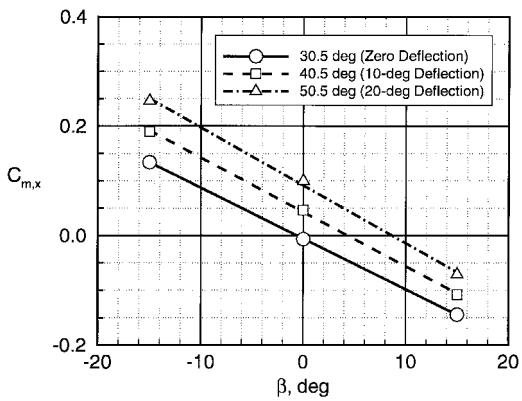

a) Moment coefficient about X axis (yaw)

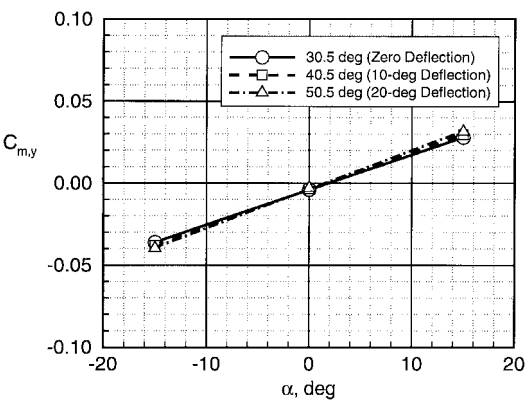

b) Moment coefficient about Y axis (pitch)

Fig. 11 Effect of $-Y$ panel deflection on aerodynamic trim.

Transitional effect on trim. In free-molecular flow, friction forces tend to constitute a larger fraction of the total force than in continuum flows. Therefore, the aerodynamic center tends to shift as a vehicle moves from free-molecular into transitional flow, and friction forces become smaller relative to pressure forces,[14] especially for blunt bodies.[15] For complex geometries that are not perfectly symmetrical about their center of mass, the trim angle may change as a function of density. The predicted variation in trim about the X and Y axes for MGS is shown in Fig. 12 for the nominal revised aerobraking configuration. The predictions show a small change in trim angle (about 0.5 deg) over this range of atmospheric densities with yaw angle β becoming more negative and pitch angle α becoming more positive.

Effect of differential ACs. Gas–surface ACs represent the degree to which incident molecules achieve equilibrium with the surface,[9] and incomplete accommodation reduces the momentum and energy transferred to the surface. For the revised aerobraking configuration, the forward facing surface of the $-Y$ panel is a completely different

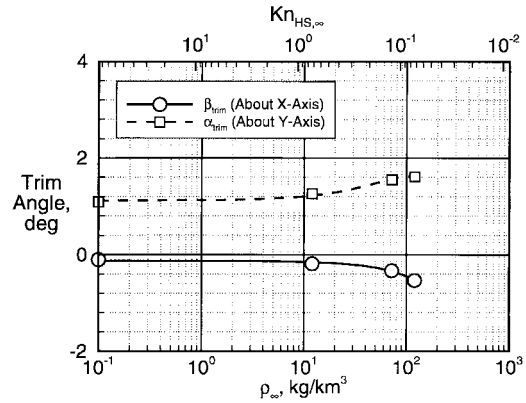

Fig. 12 Effect of atmospheric density on trim angle.

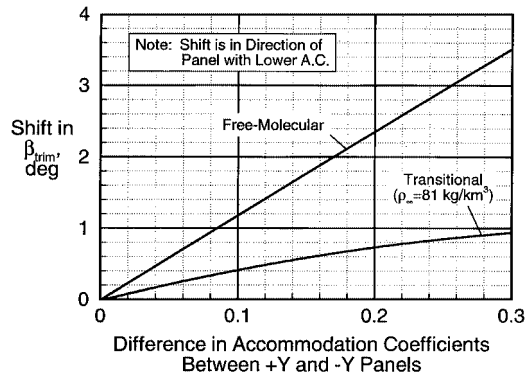

Fig. 13 Effect of differential accommodation on trim angle.

material (glass-covered solar cells) than the $+Y$ panel (composite face sheet), and the ACs are likely to be somewhat different. Although there is insufficient data to determine the exact ACs for these two materials under the Mars aerobraking conditions, limited observations with the somewhat similar Magellan spacecraft[16] suggest that differences in ACs of up to 0.2 might be possible with the $-Y$ panel having the lower AC. Therefore, DSMC and free-molecular simulations were run for various combinations of ACs on the two panels, and the effect of this differential accommodation on the trim angle β about the X axis is shown in Fig. 13. The calculations labeled "Transitional" correspond to a freestream density of $\rho_\infty = 81$ kg/km^3, which is the peak density for orbit 15 during which large $-Y$ panel deflections were observed. Lower momentum accommodation on the $-Y$ panel means there is a greater degree of specular reflection, and forces are higher in the stream direction. A moment is produced that rotates the spacecraft toward the panel with the lower AC (in this case the $-Y$ panel), which trims the spacecraft at larger yaw angles. In free-molecular flow, the predicted trim shift varies almost linearly with the difference in AC. However, in transitional flow, molecules may have multiple collisions with the surface due to being reflected back to the surface by collisions with incident freestream molecules. Therefore, the effective momentum accommodation is closer to unity in transitional flow, and the shift in trim angle is much lower. For the range of densities and differences in ACs expected for MGS, the predicted shift in trim angle is less than 2 deg in free-molecular flow and less than 1 deg for typical densities encountered at periapsis.

Flight Analysis and Results

During the aerobraking portion of orbits 12–15, the unlatched $-Y$ panel showed evidence of deflecting more than predicted based on a simple linear spring model using spring constants determined from dynamic tests performed during the MGS cruise to Mars.[7] MGS project managers decided to halt aerobraking by raising the orbit until this anomaly was thoroughly understood. Analysis of the anomaly involved a number of disciplines, e.g., structures, materials, mechanical systems, flight mechanics, aerodynamics, and the details are beyond the scope of this paper. However, rarefied aerodynamic

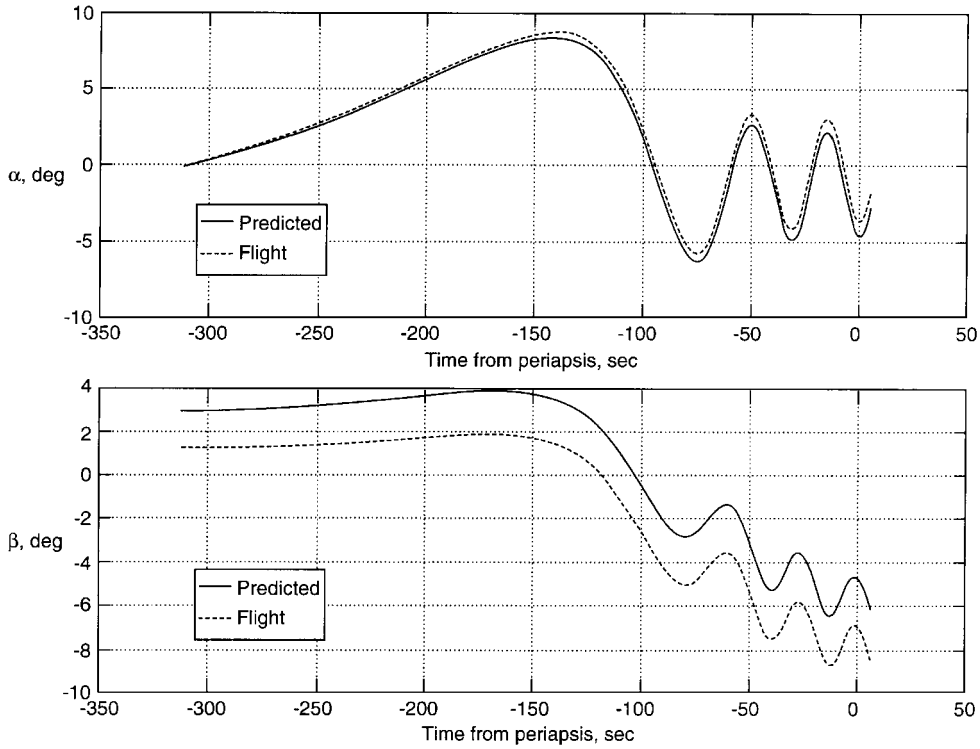

Fig. 14 Comparison of six-DOF attitude predictions to flight data for orbit 18 prior to periapsis.

predictions played an important role in the initial interpretation of panel deflections and in evaluating potential alternate aerobraking configurations that might reduce the loads on the $-Y$ panel. Other flight data analysis and observations concerning the aerothermodynamics of MGS are given by Tolson et al.[6]

Deflection of −Y Panel

Initial indication of the deflection of the $-Y$ panel came from observations of the attitude of the spacecraft. During orbits 12 and 15, the spacecraft yawed to relatively large β angles ($\approx$10 deg). Whereas some degree of yawing was expected as the $-Y$ panel deflected under aerodynamic loads, the observed yaw was greater than could be explained by deflections calculated using the simple spring model. Therefore, it was important to assess uncertainties in attitude predictions to judge the accuracy of these initial deflection estimates. The aerodynamic predictions were reviewed for sensitivity to geometry modeling, transitional effects, and differential ACs. Additional comparisons were made between the current predictions and those of the spacecraft designer that showed very good agreement under free-molecular conditions. Limited six-degree-of-freedom (DOF) trajectory simulations using techniques developed for Mars Pathfinder[17] were also performed up to the time of periapsis incorporating the current aerodynamic database. Attitude predictions from the six-DOF simulations for orbit 18 are shown in Fig. 14 and compare very well with the dynamic behavior observed from the flight data. After reviewing these various independent analyses and accounting for atmospheric rotation and winds, it was estimated that the $-Y$ panel had deflected up to 23 deg with an uncertainty of $\pm$2 deg and an uncertainty in predicted aerodynamic trim of $\pm$1 deg.

The observed deflections of the $-Y$ solar panel were later confirmed by direct measurements using sun-position sensors onboard MGS and other ancillary measurements. Structural and material analyses were also performed to develop an improved model of the damaged panel. Alternate aerobraking configurations (some of which are described in the next section) were considered as a means to alleviate some of the aerodynamic loading on the panel. Based on these various analyses, project managers developed a revised aerobraking mission that would subject the spacecraft to reduced dynamic pressures and reduced aerodynamic loads on the $-Y$ panel. Deflections of the panel continue to be monitored using sun-sensor data and aerodynamic predictions, and a comparison of observation

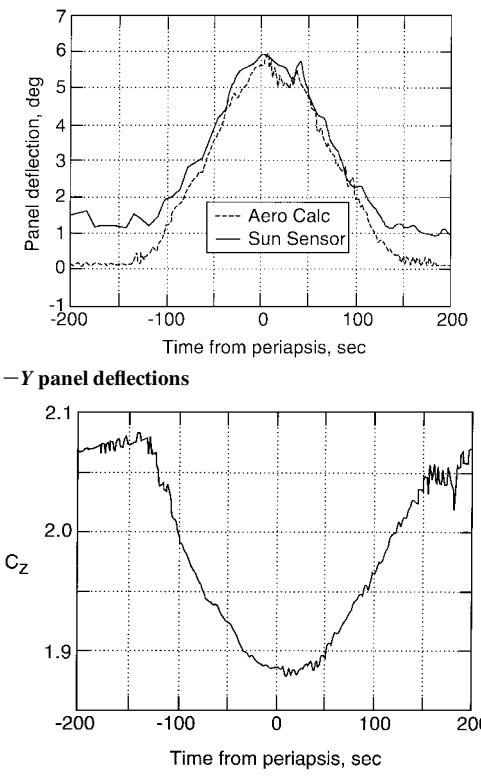

Fig. 15 Comparison of calculated deflections of $-Y$ panel with sun-sensor flight data (from Ref. 6).

and prediction for a recent aerobraking pass (from Ref. 6) at reduced dynamic pressure is shown in Fig. 15. Figure 15 also shows the variation in axial force coefficient used to extract atmospheric density from accelerometer data for this pass to demonstrate the transitional flow effect on C_z. The calculated deflections are based on the spring constant for the unlatched panel determined during cruise prior to aerobraking together with DSMC predictions of the aerodynamic hinge moments on the panel. The sun-sensor data show initial and

final offset deflections of about 1.0 to 1.5 deg, whereas the initial and final deflections are assumed to be zero in the calculations. However, the calculations are in good agreement with the deflections measured by the sun sensors during the main part of the drag pass.

Alternate Aerobraking Configurations

Alternate methods for reducing the aerodynamic loads on the partially deployed panel were considered as part of the investigation into the anomalous behavior during orbits 12–15. One approach is to alter the panel sweep angles, and the results of these alternate sweep studies demonstrate the aerobraking tradeoffs that are possible with a spacecraft like MGS. Variations in twist angle (rotating the panels about their Y axis) and sweep angle (rotating about gimbal X axis) and combinations of these rotations were investigated.

One of the more promising approaches was to sweep the $-Y$ panel backward approximately 80–85 deg to allow the inboard panel to rest against a support bracket on the spacecraft bus, thereby reducing the hinge moments on the panel. Of principal concern were the aerodynamic stability about both the X and Y axes and whether or not a net reduction in hinge moment could be obtained because a more highly swept configuration would have to fly at higher dynamic pressures to achieve the same total drag during aerobraking. These analyses were limited to a few free-molecular computations at attitudes around the estimated trim position that were sufficient to assess static stability and provide the necessary trade information. Predictions of the static aerodynamics for various sweep angles of the $+Y$ panel with the $-Y$ panel at a fixed sweep of -81 deg are shown in Fig. 16. These predictions show that the spacecraft is statically stable in pitch and yaw and show that the trim angle in yaw is approximately the bisection of the total included angle between the two swept panels. However, it should be noted that the center of mass has not been corrected to account for movement caused by sweeping the panels, although the change in center-of-mass location is expected to be small because the solar panels constitute a relatively small part of the total spacecraft mass.

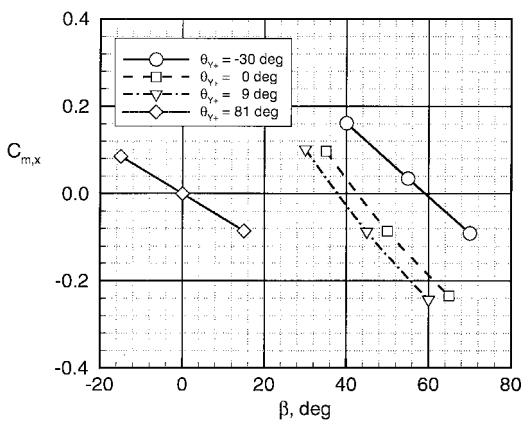

a) $C_{m,x}$ **vs** β

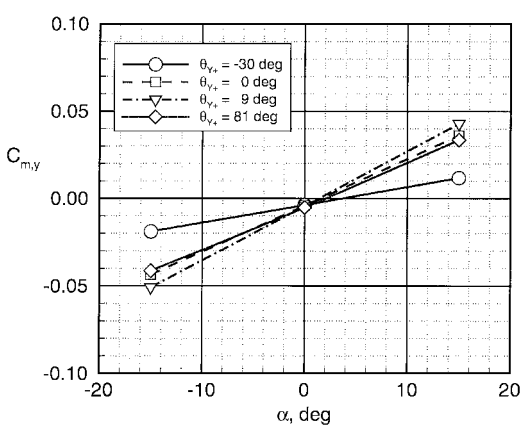

b) $C_{m,y}$ **vs** α

Fig. 16 Static aerodynamics for various sweep angles of $+Y$ panel; sweep of $-Y$ panel fixed at -81 deg.

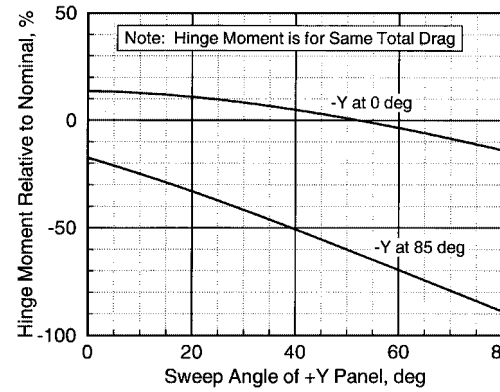

Fig. 17 Effect of $+Y$ panel sweep on $-Y$ panel hinge moment; total drag is constant.

Moments on the $-Y$ panel about the unlatched hinge axis were computed from the simulations and normalized by the total drag of the spacecraft. A plot of the normalized $-Y$ panel hinge moments expressed as a percentage difference from the normalized moment for the nominal aerobraking configuration is shown as a function of $+Y$ panel sweep angle θ_{Y+} in Fig. 17 for two different sweep angles of the $-Y$ panel. By normalizing the hinge moment to the total drag, Fig. 17 in effect shows the hinge loads for various sweep combinations that produce the same total drag. Positive values in Fig. 17 represent greater hinge loads, whereas negative values represent reduced hinge loads relative to the nominal aerobraking configuration for the same drag. For the $-Y$ panel swept to 85 deg, reductions in hinge loads of up to 90% are predicted. These more highly swept configurations would require the spacecraft to penetrate much deeper into the Mars atmosphere to achieve the same drag as the nominal design. The altered aerodynamic characteristics would also require significant changes to the flight control system. Therefore, although it was not practical to make such changes for the MGS mission, these predictions emphasize that aerobraking is an aerodynamic mission, and flying through planetary atmospheres may warrant more detailed assessment of the aerodynamic characteristics of future aerobraking spacecraft.

Conclusion

DSMC and free-molecular methods have been used to provide aerothermodynamic predictions for the MGS from design through aerobraking flight. The predictions were used to design thermal protection, optimize aerobraking trajectories, provide data for mission planning, interpret flight results, and provide operational support. MGS is the first planetary mission in which rarefied flow predictions have played such an integral role.

The results demonstrate the capabilities of current three-dimensional DSMC and free-molecular codes to model rarefied flows about complex spacecraft geometries, and good agreement between two different DSMC codes is shown. Heating predictions show significant rarefied transitional flow effects on the MGS solar panels with significantly higher heating near the edges of the panel than at their centers. Drag predictions also show significant reduction of the aerodynamic drag coefficient at the highest densities that MGS is expected to encounter. The MGS aerobraking configuration is shown to be aerodynamically stable, and good agreement is obtained between various prediction techniques.

Off-nominal behavior caused by an unlatched solar panel presented a challenge to redefine the aerodynamic properties of MGS while the spacecraft was cruising to Mars. Further challenges were presented to interpret the attitude behavior of the spacecraft when aerobraking began. The current state of three-dimensional rarefied flow prediction tools is such that these challenges could be met with sufficient confidence to assist mission planners in a real-time manner.

Aerothermodynamic predictions continue to play an important role in monitoring the state of the MGS spacecraft and in extracting

new information on the atmospheric structure of Mars. The results obtained and the lessons learned will benefit future Mars missions and aerobraking maneuvers to other planets.

Acknowledgments

Prasun Desai and Richard Powell, NASA Langley Research Center, performed the six-degree-of-freedom simulations of Mars Global Surveyor (MGS) using the predicted aerodynamic database. George Cancro, George Washington University, provided analysis and comparisons of panel deflections and flight data from sun sensors. Gary Qualls, NYMA, Inc., provided structural analysis of solar panel deflections. William Willcockson, Lockheed-Martin Corp., provided extensive information on MGS geometry, mission operations, and flight data.

References

[1]Dallas, S. S., "Mars Global Surveyor Mission," *Proceedings of 1997 IEEE Aerospace Conference*, Inst. of Electrical and Electronics Engineers, New York, 1997, pp. 173–189.

[2]Lyons, D., "Aerobraking Magellan: Plan Versus Reality," American Astronautical Society, AAS Paper 94-118, Feb. 1994.

[3]Rault, D. F., Cestero, F. J., and Shane, R. W., "Spacecraft Aerodynamics During Aerobraking Maneuver in Planetary Atmospheres," AIAA Paper 96-1890, June 1996.

[4]Rault, D. F., "RCS Plume Effect on Spacecraft Aerodynamics During Aerobraking Maneuver," *Rarefied Gas Dynamics 20*, edited by C. Shen, Peking Univ. Press, Beijing, PRC, 1996, pp. 549–554.

[5]Shane, R. W., Rault, D. F., and Tolson, R. H., "Mars Global Surveyor Aerodynamics for Maneuvers in Martian Atmosphere," AIAA Paper 97-2509, June 1997.

[6]Tolson, R. H., Keating, G. M., Cancro, G. J., Parker, J. S., Noll, S. N., and Wilkerson, B. L., "Application of Accelerometer Data to Mars Global Surveyor Aerobraking Operations," *Journal of Spacecraft and Rockets*, Vol. 36, No. 3, 1999, pp. 323–329.

[7]Lyons, D., "Mars Global Surveyor: Aerobraking with a Broken Wing," American Astronautical Society, AAS Paper 97-618, Aug. 1997.

[8]Lyons, D. T., Beerer, J. G., Esposito, P., Johnston, M. D., and Willcockson, W. H., "Mars Global Surveyor: Aerobraking Mission Overview," *Journal of Spacecraft and Rockets*, Vol. 36, No. 3, 1999, pp. 307–313.

[9]Bird, G. A., *Molecular Gas Dynamics and the Direct Simulation of Gas Flows*, Clarendon, Oxford, England, UK, 1994.

[10]Borgnakke, C., and Larsen, P. S., "Statistical Collision Model for Monte Carlo Simulation of Polyatomic Gas Mixture," *Journal of Computational Physics*, Vol. 18, No. 4, 1975, pp. 405–420.

[11]Rault, D. F., "Efficient Three-Dimensional Direct Simulation Monte Carlo Code for Complex Geometry Problems," *Rarefied Gas Dynamics: Theory and Simulations*, edited by B. D. Shizgal and D. P. Weaver, Vol. 160, Progress in Astronautics and Aeronautics, AIAA, Washington, DC, 1994, pp. 137–154.

[12]Wilmoth, R. G., LeBeau, G. J., and Carlson, A. B., "DSMC Grid Methodologies for Computing Low-Density Hypersonic Flows About Reusable Launch Vehicles," AIAA Paper 96-1812, June 1996.

[13]Shane, R. W., "Aerothermodynamics of the Mars Global Surveyor Spacecraft," M.S. Thesis, Joint Inst. for Advancement of Flight Sciences, George Washington Univ., Hampton, VA, Dec. 1997.

[14]Dogra, V. K., and Moss, J. N., "Hypersonic Rarefied Flow About Plates at Incidence," *AIAA Journal*, Vol. 29, No. 8, 1991, pp. 1250–1258.

[15]Moss, J. N., Blanchard, R. C., Wilmoth, R. G., and Braun, R. D., "Mars Pathfinder Rarefied Aerodynamics: Computations and Measurements," AIAA Paper 98-0298, Jan. 1998.

[16]Espiritu, R. C., and Tolson, R. H., "Determining Venusian Upper Atmosphere Characteristics Using Magellan Attitude Control Data," American Astronautical Society, AAS Paper 95-152, Feb. 1995.

[17]Braun, R. D., Powell, R. W., Engelund, W. C., Gnoffo, P. A., Weilmuenster, K. J., and Mitcheltree, R. A., "Mars Pathfinder Six-Degree-of-Freedom Entry Analysis," *Journal of Spacecraft and Rockets*, Vol. 32, No. 6, 1995, pp. 993–1000.

R. D. Braun
Guest Editor